Contents lists available at ScienceDirect

Digital Chinese Medicine

journal homepage: http://www.keaipublishing.com/dcmed

Mechanism of electroacupuncture treating detrusor-bladder neck dyssynergia after suprasacral spinal cord injury by proteomics

Liya TANG[a†], Qirui QU[a†], Jincan LIU[a], Ming XU[a], Lu ZHOU[b], Qiong LIU[a], Kun AI[a*]

a. School of Acupuncture, Tuina and Rehabilitation, Hunan University of Chinese Medicine, Changsha, Hunan 410208, China

b. Department of Rehabilitation Medicine, Chenzhou First People's Hospital, Chenzhou, Hunan 423000, China

ARTICLE INFO

Article history
Received 22 December 2024
Accepted 14 May 2025
Available online 25 June 2025

Keywords
Electroacupuncture
Suprasacral spinal cord injury
Detrusor-bladder neck dyssynergia
Detrusor
Bladder neck
Proteomics analysis
Differentially expressed proteins

ABSTRACT

Objectives To elucidate the potential mechanisms of electroacupuncture (EA) in restoring detrusor-bladder neck dyssynergia (DBND) following suprasacral spinal cord injury (SSCI).

Methods A total of 52 specific pathogen-free (SPF) grade famale Sprague-Dawley (SD) rats (10 – 12 weeks, 250 – 280 g) were randomly assigned to either a sham group (n = 12) or a spinal cord injury model group (n = 40). In the model group, DBND was induced through Hassan Shaker spinal cord transection at T10 level, with 24 rats meeting inclusion criteria and subsequently randomized into DBND group (n = 12) and EA intervention group (DBND + EA group, n = 12). After spinal shock recovery (day 19 after modeling), DBND + EA group received EA treatment at Ciliao (BL32), Zhongji (RN3), and Sanyinjiao (SP6) acupoints for 20 min per session at 10/50 Hz frequencies, once daily for 10 d. Sham and DBND groups received anesthesia only without EA intervention. On day 29 post-modeling, all rats underwent urodynamic assessments, followed by hematoxylin and eosin (HE) staining, tandem mass tag (TMT) proteomics, and Western blot (WB) analysis of detrusor and bladder neck tissues. Differentially expressed proteins (DEPs) were defined as proteins with $P < 0.05$, unique peptides $\geqslant 2$, and fold change > 1.2 or < 0.83. Kyoto Encyclopedia of Genes and Genomes (KEGG) pathway analysis was performed using KOBAS 3.0 ($P < 0.01$), and protein-protein interaction (PPI) networks were analyzed using Search Tool for the Retrieval of Interacting Genes/Proteins (STRING) 11.5 and Cytoscape 3.9.1.

Results Compared with sham group, DBND group showed significantly elevated leak point pressure (LPP) and maximum cystometric capacity (MCC) (both $P < 0.01$). EA treatment significantly reduced both LPP and MCC compared with DBND group ($P < 0.01$ and $P < 0.05$, respectively). HE staining revealed that EA reduced detrusor fibrosis and improved bladder neck inflammation. TMT proteomics identified 30 overlapping DEPs in detrusor and 59 overlapping DEPs in bladder neck when comparing DBND + EA/DBND groups with sham group. In detrusor tissue, KEGG analysis revealed 10 significantly enriched pathways ($P < 0.01$), including mitogen-activated protein kinase (MAPK) signaling pathway. PPI analysis showed 22 of 30 DEPs were interconnected. In bladder neck tissue, 14 pathways were significantly enriched ($P < 0.01$), including relaxin signaling pathway, with 51 of 59 DEPs showing interconnections. Both TMT and WB validations demonstrated that compared with sham controls, DBND rats exhibited upregulated collagen type IV alpha 2 chain (Col4a2) and downregulated

†The authors contributed equally.

*Corresponding author: Kun AI, E-mail: aikun650@qq.com.

Peer review under the responsibility of Hunan University of Chinese Medicine.

DOI: 10.1016/j.dcmed.2025.05.011

Citation: TANG LY, QU QR, LIU JC, et al. Mechanism of electroacupuncture treating detrusor-bladder neck dyssynergia after suprasacral spinal cord injury by proteomics. Digital Chinese Medicine, 2025, 8(2): 267-278.

guanine nucleotide-binding protein G(z) subunit alpha (Gnaz) in detrusor tissue, while EA treatment normalized both proteins (both $P < 0.05$). In bladder neck tissue, DBND rats showed decreased expression of smoothelin (Smtn) and calcium-activated potassium channel subunit beta-1 (Kcnmb1) compared with sham controls (both $P < 0.01$), which were both upregulated following EA treatment ($P < 0.01$ and $P < 0.05$, respectively).

Conclusion EA restores detrusor-bladder neck coordination in DBND through dual-target mechanisms. In detrusor tissue, EA modulates contraction via extracellular matrix remodeling, cyclic adenosine monophosphate (cAMP) signaling pathway regulation, and enhanced adenosine triphosphate (ATP) biosynthesis mediated by neurotransmitters. In bladder neck tissue, EA promotes relaxation by maintaining contractile phenotypes, reducing fibrosis, suppressing smooth muscle excitation, and regulating presynaptic neurotransmitter release. These findings provide mechanistic insights into EA's therapeutic role in managing DBND.

1 Introduction

Neurogenic bladder is a common complication after suprasacral spinal cord injury (SSCI). According to a 2024 study, approximately 71.8% of patients with spinal cord injury (SCI) had bladder dysfunction [1]. The urinary function of the bladder is controlled by the bladder detrusor muscle, the bladder neck, and the external urethral sphincter. During normal bladder emptying, the parasympathetic nerve (S2 – S4) in the spinal cord is activated, which causes bladder detrusor contraction. Furthermore, inhibition of the sympathetic nerves innervating the bladder neck (T11 – L2) and the somatic nerves innervating the external urethral sphincter (controlled by Onuf's nucleus at S2 – S4) results in bladder neck dilation, urethral relaxation, and urination. With SCI at T10 and above, the sympathetic and parasympathetic nerves innervating the bladder become disconnected from the pons and other higher urination centers, which results in autonomic dysreflexia (AD). In AD patients with SSCI, sympathetic overactivity leads to impaired bladder detrusor contractility and bladder neck overcontraction [2]. During urination, the detrusor and bladder neck are coordinated abnormally in a condition known as detrusor-bladder neck dyssynergia (DBND) [3]. If not treated in time, DBND may lead to urinary retention, urine reflux, kidney failure, and other serious urinary problems [4].

Therefore, DBND needs to be considered and addressed in the clinic. Alleviating excessive bladder neck contraction, promoting effective detrusor contraction, and applying dual-target interventions that address both issues should be the main clinical approaches to improve DBND after SSCI. Currently, most DBND treatments are targeted solely at the bladder neck, with few reports on dual-target treatments addressing both the bladder neck and detrusor. In clinical practice, DBND is mainly treated by surgery, intermittent catheterization, and α-adrenergic blockers for the bladder neck, whereas there are few effective interventions for the bladder detrusor [5]. The current treatment methods have achieved some degree of clinical efficacy. However, they tend to address single therapeutic targets, and postoperative complications, drug side effects, and other shortcomings accompany them.

Electroacupuncture (EA) is widely used to treat DBND because of its low invasiveness, lack of drug side effects, and confirmed efficacy [6]. Study has shown that acupuncture can bidirectionally regulate the function of diseased regions to restore a normal physiological state [7]. After patients with sphincter hyperactivity underwent acupuncture treatment, the bladder output increased, residual urine volume and bladder pressure decreased [8]. Additionally, in patients with detrusor hyperreflexia, acupuncture can increase the maximum bladder volume and reduce the frequency of urination [9]. These studies also suggest that acupuncture has a multitarget therapeutic effect, and the internal mechanism of acupuncture treatment for DBND likely involves the regulation of the detrusor and bladder neck. At present, research on the mechanism by which acupuncture treats neurogenic bladder mainly focuses on improving bladder detrusor function and the external urethral sphincter, or alleviating the loss of local spinal cord neurons [10]. In our study of EA as a treatment for DBND, we considered studies observing both the detrusor muscle and the bladder neck.

Proteins are the main molecules that carry out biological activities. Studies have shown that protein expression changes in spinal cord injury-induced neurogenic bladder [11]. Tandem mass tag (TMT) technology is a quantitative proteomics tool that can comprehensively detect proteins expressed in tissues. Quantitative proteomics analysis has not been used to research the potential mechanism of EA treating DBND after SSCI with detrusor muscle and bladder neck as dual therapeutic targets.

Therefore, in this study, we established a DBND rat model by transection of the T10 spinal cord segment, and used TMT quantitative proteomics method, combined with bioinformatics analysis and Western blot (WB), to

investigate the mechanism of EA in regulating detrusor contraction and bladder neck coordination to improve voiding function in SSCI-induced DBND.

2 Materials and methods

2.1 Animal sources and initial grouping

A total of 52 specific pathogen-free (SPF) grade female Sprague-Dawley (SD) rats (10 – 12 weeks, 250 – 280 g) were procured from Hunan Slack Jingda Experimental Animal Co., Ltd. (Certification No. 1107271911006889) through Hunan University of Chinese Medicine Animal Center [No. SYXK (Xiang) 2019-0009], with ethical approval (No. LL2019092303) from the Institutional Animal Care and Use Committee. Animals were maintained at 24 – 26 °C and 50% – 70% humidity under 12 h/12 h light cycles with free access to food and water, followed by 7-d acclimatization before experiments. Among the 52 rats, 12 were assigned to the sham group, and the remaining rats were assigned to the model group.

2.2 Modeling

The rats in model group were subjected to T10 spinal cord injury using the Hassan Shaker spinal cord transection method [12]. After 7 d of routine feeding, the model group rats were fasted and given water for 24 h. The rats were anesthetized by intraperitoneal injection of 3% sodium pentobarbital at a dose of 50 mg/kg (Merck KGaA, USA). The rats were fixed in the supine position, and the 13th thoracic vertebra was used as a bony marker. Rats' subcutaneous tissue at the 8th to 9th thoracic vertebrae was dissected longitudinally, separating the musculature on both sides of the spine, removing T8 and T9 spinous processes and vertebral arches, exposing the spinal cord, cutting off the spinal cord with No. 11 surgical blade, then suturing the muscles, sterilizing the incision and its surroundings with 5% compound iodine, and suturing the skin.

In the sham group, the skin above the 8th and 9th thoracic vertebrae was incised to expose the spinal cord, but the spinal cord was not transected. The Crede maneuver was used to assist voiding daily at 6:00, 14:00, and 22:00.

2.3 Animal model evaluation

The T10 spinal cord injury model was evaluated after spinal shock (day 18 after modeling) by observing the hindlimb motor and bladder voiding function. A complete SSCI model was considered successful when the rat exhibited total hindlimb dragging during locomotion and achieved a Basso-Beattie-Bresnahan (BBB) locomotor score of 0 [13].

Among the SSCI rats, DBND rats were further selected. The rats were still unable to urinate spontaneously and retained urine after the bladder shock phase. Resistance to urine outflow from the urethral orifice was also observed during manual urine expression. If these conditions were met, the DBND model was considered successfully established.

2.4 Model-compliant animal regrouping

Among the 40 rats initially assigned to the modeling group, 10 rats succumbed during the spinal shock period. Post-spinal shock, 3 rats exhibited spontaneous hindlimb motor activity, and 3 demonstrated spontaneous micturition. The remaining 24 rats met the model standard and were randomly assigned to DBND group (n = 12) and DBND + EA group (n = 12).

2.5 Intervention

Rats in DBND + EA group were treated with EA (20 min per session, once daily for 10 d) after model evaluation (day 19 after modeling). The dimensions of the acupuncture needles were 0.30 mm × 25 mm (Huatuo brand, China). The DBND was treated with EA at Ciliao (BL32), Zhongji (RN3), and Sanyinjiao (SP6) [10]. The needle insertion depths at these three points were 10 mm, 5 mm, and 5 mm, respectively. Rats in DBND + EA group underwent induction anesthesia with 4% isoflurane (0.8 L/min) and were secured to a rat board for EA intervention. Anesthesia was maintained with 2% isoflurane (0.6 L/min) throughout the procedure. The following parameters were used for EA stimulation: a density wave, frequencies of 10/50 Hz, and intensity that caused limb tremor while remaining tolerable. Rats in sham and DBND groups received isoflurane inhalation anesthesia exclusively, serving as non-EA control groups in the experimental design.

2.6 Test methods

2.6.1 Urodynamics tests After EA intervention for 10 d, all rats were anesthetized with 3% sodium pentobarbital at a dose of 50 mg/kg. Then, the rats were fixed in the supine position with no urine in the bladder, and a urinary catheter was inserted into the bladder, and 0.9% normal saline (25 – 35 °C) was infused intravesically (100 μL/min). Finally, bladder pressure curve changes, maximum cystometric capacity (MCC), and leak point pressure (LPP) were recorded using an MP150 multichannel physiological recorder (Biopac, USA).

2.6.2 HE staining After urodynamics, rats were anesthetized and euthanized immediately using 5% sodium pentobarbital. Normal saline was rapidly injected through the left ventricle for perfusion until the outflowing

fluid became clear, after which 4% paraformaldehyde was injected into the ventricle for perfusion fixation. Standardized detrusor and bladder neck specimens (0.5 cm × 0.5 cm) were harvested on ice. After 48 h of fixation with 4% paraformaldehyde, the detrusor and bladder neck were dehydrated through 70%, 80%, 95%, and 100% ethanol (1 h per step), embedded in paraffin (58 – 60 °C), and sectioned (5 μm). Sections were mounted on slides, baked (60 °C for 2 h), deparaffinized in xylene I and II (10 min each), and rehydrated. Hematoxylin staining (Harris, 8 min) with 1 min water rinse was followed by 0.5% acid alcohol differentiation (10 s) and bluing in running water (30 min). Tissue sections were counterstained with 0.5% alcoholic eosin Y (3 min), dehydrated in ethanol (95% and 100%, 2 × 5 min each), cleared in xylene I, II, and III (5 min each), and mounted with neutral resin. Micromorphology of the detrusor and bladder neck was observed under a light microscope.

2.6.3 TMT quantitative proteomics analysis (i) TMT labeling. TMT labeling and proteomic analyses were performed by Aksomics, Inc. (Shanghai, China). Proteomic profiling was conducted using TMT10-plex isobaric labeling (Thermo Scientific, Cat# 90 110) on an Orbitrap Exploris™ 480 mass spectrometer coupled to a nanoElute® UPLC system (Bruker). Detrusor and bladder neck tissues from three randomly selected rats per group were homogenized in radioimmunoprecipitation assay lysis (RIPA) buffer, centrifuged (12 000 × g, 15 min, 4 °C), and 100 μg protein lysate per sample underwent reduction (10 mmol/L DTT), alkylation (55 mmol/L IAA), tryptic digestion (1 : 50 w/w, 16 h), and TMT labeling. Database searches against UniProt Rat proteome (2023_01 release, 8 124 entries) utilized Proteome Discoverer 3.0 with parameters: trypsin cleavage (maxium 2 missed cleavages), 10 ppm/0.02 Da mass tolerance (MS1/MS2), fixed carbamidomethyl modification (C), variable oxidation (M) and N-terminal acetylation, and TMT10plex modifications. TMT quantification employed reference channel (131C)-normalized median intensity scaling, requiring ⩾ 2 unique peptides per protein and 70% valid value rate across replicates.

(ii) Proteomic analysis. MaxQuant (v1.6.1.0) was used for database searches and TMT-based quantitative analysis of the raw data obtained by LC–MS/MS analysis. The protein database was UniProt_Rattus_20190711_ISO. The false discovery rate (FDR) levels for polypeptides and proteins were controlled at 0.01. The 10 samples were normalized to make each group's total protein content or median consistent. Proteins with $P < 0.05$, unique peptides ⩾ 2, and fold change (FC) > 1.2 or < 0.83 were defined as differentially expressed proteins (DEPs) [14].

(iii) Bioinformatics analysis of DEPs. KOBAS v3.0 (http://kobas.cbi.pku.edu.cn/) was used for Kyoto Encyclopedia of Genes and Genomes (KEGG) pathway analysis (using *Rattus norvegicus* database, $P < 0.01$) [15]. Subsequently, the enrichment results were sorted according to the input number, and the top 10 ($P < 0.01$) and 14 KEGG pathways ($P < 0.01$) were screened for detrusor and bladder neck, respectively. Search Tool for the Retrieval of Interacting Genes/Proteins (STRING) v11.5 (https://string-db.org/) and Cytoscape v3.9.1 were used to construct protein-protein interaction (PPI) analysis networks [16, 17].

2.6.4 WB protocol A total of 30 DEPs in the detrusor muscle and 59 DEPs in the bladder neck were identified and retrieved from PubMed database. After screening DEPs associated with detrusor or bladder neck functions, we randomly selected two DEPs from detrusor or bladder neck for WB validation to assess whether their expression patterns aligned with TMT. Detrusor and bladder neck tissues were lysed and centrifuged before determination with the bicinchoninic acid (BCA) quantification kit (Thermo Scientific, USA). A certain amount of protein stock solution was thoroughly mixed with 4 × loading buffer and then denatured in a boiling water bath. Protein samples were separated by 8% or 10% sodium dodecyl sulfate-polyacrylamide gel electrophoresis (SDS-PAGE) and transferred to 0.45 μm polyvinylidene fluoride (PVDF) membranes. Then, the PVDF membranes were blocked in 5% skim milk solution. Membranes were incubated with rabbit anti-Col4a2 (1 : 1 000, Abclonal, China), rabbit anti-guanine nucleotide-binding protein G(z) subunit alpha (Gnaz) (1 : 1 000, Abclonal, China), rabbit anti-Kcnmb1 (1 : 1 000, Thermo Fisher Scientific, USA), rabbit anti-Smtn (1 : 1 000, Abclonal, China), and mouse anti-β-actin (1 : 8 000, Abcam, UK) overnight at 4 °C. Goat anti-rabbit IgG secondary antibody (1 : 10 000, Elabscience, China) or goat anti-mouse IgG secondary antibody (1 : 10 000, Elabscience, China) was added and incubated at 37 °C for 1 h. Finally, the PVDF membrane was incubated with freshly prepared enhanced chemiluminescence (ECL) solution (Advansta, USA) for 2 min. PVDF membranes were imaged using a chemiluminescence system (Bio-Rad ChemiDoc XRS+), with protein band intensities quantified via ImageJ software to determine target protein/β-actin expression ratios.

2.7 Statistical analysis

SPSS 26.0 statistical software was used for analysis, and data were expressed as mean ± standard deviation (SD). One-way analysis of variance (ANOVA) was used to compare groups, and a *t* test was used to compare pairs. $P < 0.05$ was considered statistically significant.

3 Results

3.1 EA ameliorating urinary dysfunction in DBND after SSCI

The rats in sham group were in good general condition. In DBND and DBND + EA groups, all voluntary hind limb movement disappeared after spinal shock, and the rats

moved by dragging themselves. The bladder was enlarged in the lower abdomen during palpated. The lower abdomens of the rats and cage lining pads were slightly damp, and resistance was felt during manual urination. After EA intervention, the degrees of bladder distension and resistance to manually assisted urination in DBND + EA group were reduced. Figure 1A shows that daily manually assisted urine output in DBND group fluctuated wildly after spinal cord shock, while DBND + EA group showed a slight downward trend. Compared with sham group, urodynamics revealed that LPP and MCC in DBND group were significantly increased ($P < 0.01$). LPP and MCC in the DBND + EA were significantly decreased after EA intervention ($P < 0.01$ and $P < 0.05$, respectively) (Figure 1B and 1C). HE staining showed that the detrusor mucosa of DBND group had focal shedding of the mucosal epithelium, enlarged smooth muscle nuclei, muscle fiber hypertrophy, smooth muscle wall thickening, and collagen fiber hyperplasia in the muscle layer. EA treatment markedly reduced these anomalies (Figure 1D). In addition, a mass of fibroblasts and inflammatory cells infiltrated the lamina propria of the bladder neck in DBND group, smooth muscle cell nuclei were enlarged and muscle fibers were thickened. EA significantly improved the pathologic changes of the bladder neck (Figure 1E). These results indicate that EA can ameliorate urinary dysfunction in DBND after SSCI.

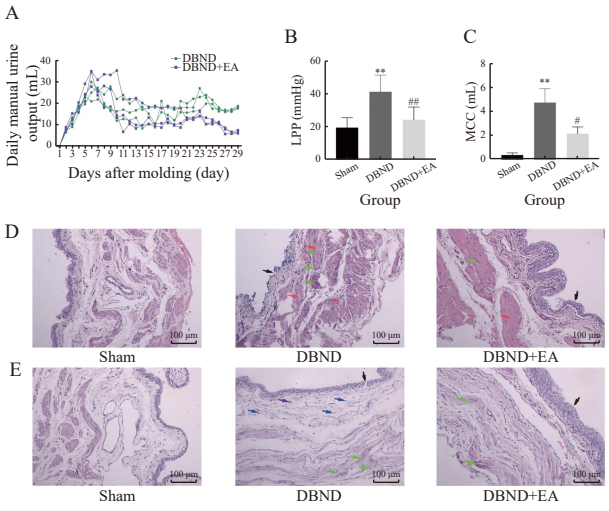

Figure 1 Therapeutic effects of EA on DBND

A, daily manual-assisted urine output. B, LPP. C, MCC. D, morphological changes of the bladder detrusor in different groups (× 10). E, morphological changes of the bladder neck in different groups (× 10). $^{**}P < 0.01$, compared with sham group. $^{\#}P < 0.05$ and $^{\#\#}P < 0.01$, compared with DBND group. Black arrow, focal shedding of the mucosal epithelium. Green arrow, enlarged smooth muscle nuclei. Red arrow, collagen fiber hyperplasia. Blue arrow, fibroblasts. Purple arrow, inflammatory cells.

3.2 TMT quantitative proteomic analysis of the detrusor

3.2.1 TMT analysis of DEPs Detrusor TMT results showed that a total of 4 470 quantifiable proteins were detected. A total of 230 DEPs (126 up-regulated, 104 down-regulated) were present in sham/DBND groups (Figure 2A). A total of 172 DEPs (93 up-regulated and 79 down-regulated) were observed in DBND + EA/DBND groups (Figure 2B). A total of 30 overlapping DEPs were found between sham/DBND groups and DBND + EA/DBND groups (Figure 2C). In DBND + EA group, EA reversed 29 overlapping DEPs, and 1 overlapping DEP was consistent with DBND group (Supplementary Table S1).

3.2.2 KEGG pathway analysis of DEPs KEGG pathway enrichment analysis was performed on the 30 DEPs, and 10 pathways were significantly enriched ($P < 0.01$). Among the 30 DEPs, p21-activated kinase 1 (Pak1) and microtubule-associated protein tau (Mapt) were implicated in the mitogen-activated protein kinase (MAPK) signaling pathway, syndecan-4 (Sdc4) and Pak1 in proteoglycans in cancer, collagen type IV alpha 2 chain (Col4a2) and Pak1 in focal adhesion, Pak1 and actin binding LIM protein family member 2 (Ablim2) in axon guidance, Sdc4 and intercellular adhesion molecule 1 (Icam1) in cell adhesion molecules as well as fluid shear stress and atherosclerosis, Col4a2 and Icam1 in the advanced glycation end products-receptor for advanced glycation end products (AGE-RAGE) signaling pathway in diabetic complications, Pak1 and Icam1 in natural killer cell-mediated cytotoxicity, Sdc4 and Col4a2 in ECM-receptor interaction, and Gnaz in long-term depression (Figure 2D).

3.2.3 PPI analysis of DEPs PPI analysis was performed for 30 DEPs, revealing a network of interacting proteins. In the PPI network, each node represents a DEP, and each edge indicates a functional or physical interaction between DEPs. Among the 30 DEPs analyzed, 22 were found to be interconnected. The darker the node's color, the more edges are connected to the DEPs within the network. Network analysis identified albumin (Alb), microtubule-associated protein tau (Mapt), and insulin-like growth factor-binding protein 5 (Igfbp5) as the most extensively interconnected nodes within this DEPs interaction network (Figure 2E).

3.3 TMT quantitative proteomic analysis of the bladder neck

3.3.1 TMT analysis of DEPs Bladder neck TMT results showed that 4 392 quantifiable proteins were detected. A total of 614 DEPs (306 up-regulated, 308 down-regulated) were present in sham/DBND groups (Figure 3A). A total of 135 DEPs (56 up-regulated and 79 down-regulated) were present in DBND + EA/DBND groups (Figure 3B). 59 overlapping DEPs were found in sham/DBND groups and DBND + EA/DBND groups (Figure 3C). In DBND

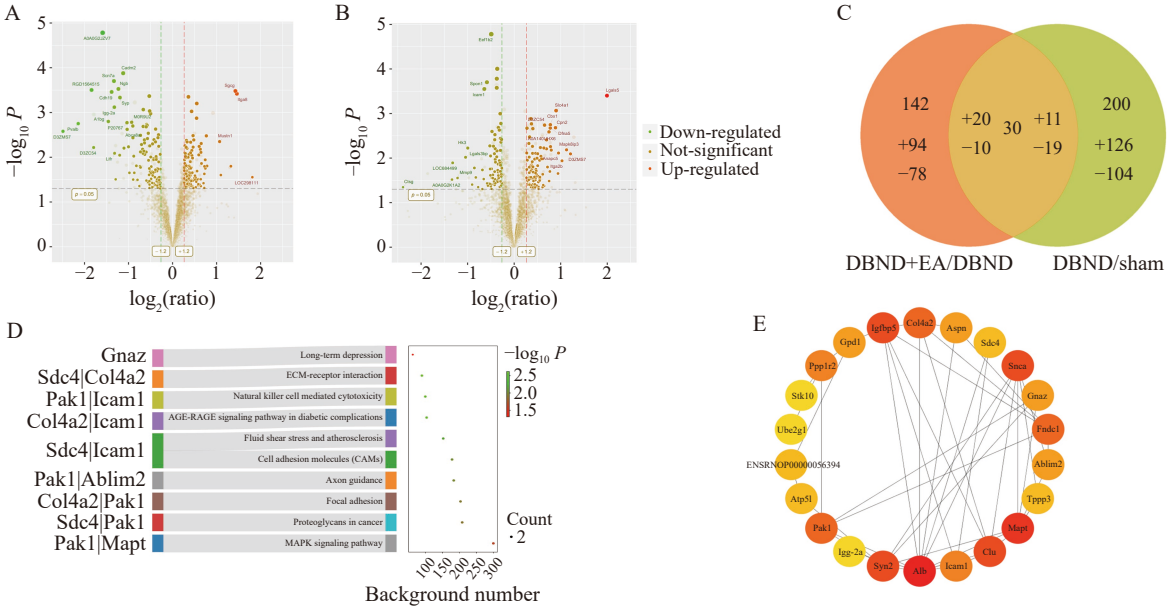

Figure 2 TMT quantitative proteomic analysis of bladder detrusor

A, volcano map of DBND/sham groups with 230 DEPs. B, volcano map of DBND + EA/DBND groups with 172 DEPs. C, Venn plot of DEPs and 30 overlapping proteins between DBND/sham groups and DBND + EA/DBND groups. " + " represents up-regulated DEPs and "–" represents down-regulated DEPs. D, KEGG pathway map of 30 DEPs. E, PPI network plot of 30 DEPs.

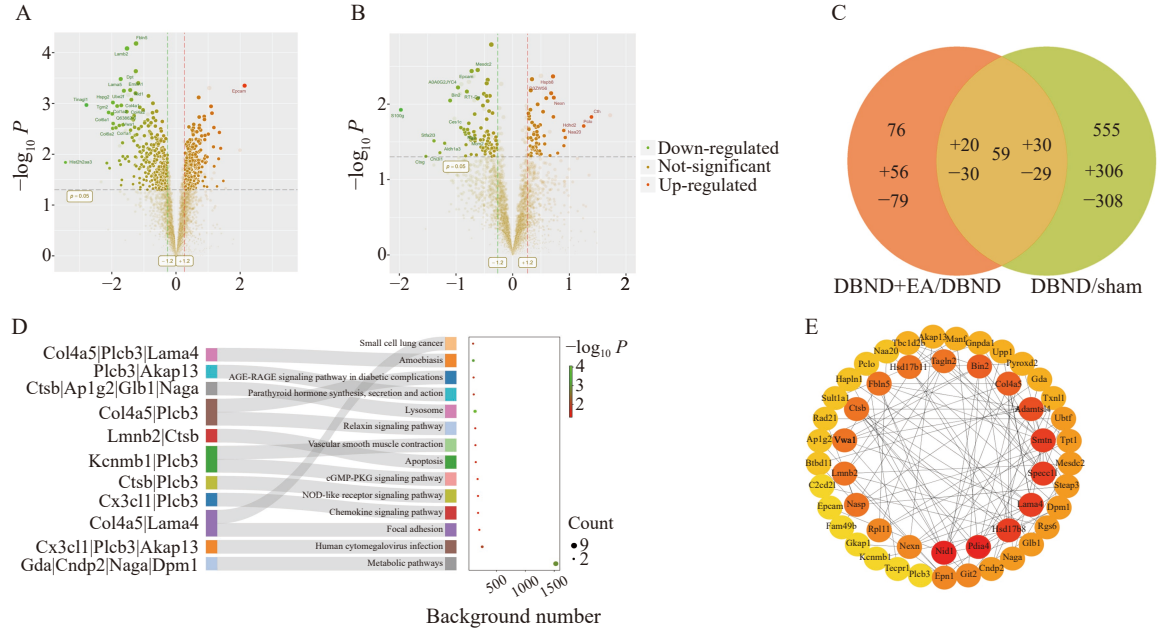

Figure 3 TMT quantitative proteomic analysis of the bladder neck

A, volcano map of DBND/sham groups with 614 DEPs. B, volcano map of DBND + EA/DBND groups with 135 DEPs. C, Venn plot of DEPs and 59 overlapping proteins between DBND/sham groups and DBND + EA/DBND groups. " + " represents up-regulated DEPs and "–" represents down-regulated DEPs. D, KEGG pathway map of 59 DEPs. E, PPI network plot of 59 DEPs.

group, 59 overlapping DEPs were reversed by EA (Supplementary Table S2).

3.3.2 KEGG pathway analysis of DEPs KEGG pathway enrichment analysis was performed on 59 DEPs, and 14 pathways were significantly enriched ($P < 0.01$). Among the 59 DEPs, Col4a5, Plcb3, and Lama4 were associated with the amoebiasis; Plcb3 and Akap13 participated in the parathyroid hormone synthesis, secretion, and action; Ctsb, Ap1g2, Glb1, and Naga were involved in the lysosome; Col4a5 and Plcb3 were linked to the AGE-RAGE signaling pathway in diabetic complications and relaxin signaling pathway; Lmnb2 and Ctsb contributed to the apoptosis; Kcnmb1 and Plcb3 played roles in the vascular smooth muscle contraction and the cGMP-PKG signaling pathway; Ctsb and Plcb3 were part of the NOD-like receptor signaling pathway; Cx3cl1 and Plcb3 were connected to the chemokine signaling pathway; Col4a5

and Lama4 were related to the small cell lung cancer and focal adhesion; Cx3cl1, Plcb3 and Akap13 were associated with the human cytomegalovirus infection; and Gda, Cndp2, Naga, and Dpm1 were involved in the metabolic pathways (Figure 3D).

3.3.3 PPI analysis of DEPs The interactions of 59 proteins are shown in the PPI network. Each node in the PPI network represents a differentially expressed protein. The edges represent PPI among DEPs, with 51 out of 59 DEPs demonstrating interconnected relationships. The darker the color of the node, the more edges are connected to the DEPs. Network analysis revealed nidogen-1 (Nid1), protein disulfide-isomerase A4 (Pdia4), and (3R)-3-hydroxyacyl-CoA dehydrogenase (Hsd17b8) as the most extensively interconnected nodes within this DEP interaction network (Figure 3E).

3.4 WB confirmation of TMT-based results

We performed a literature review to examine the function of the 30 DEPs in the detrusor and the 59 DEPs in the bladder neck. In detrusor, we found that Col4a2 ultimately affects the contraction of detrusor through the ECM-receptor interaction pathway and focal adhesion pathway [18]. Gnaz affects the contraction of smooth muscle cells by regulating adenylate cyclase (AC)/cyclic adenosine monophosphate (cAMP)/myosin phosphatase target subunit 1 (MYPT1)/myosin light chain (MLC) signaling pathways [19], insulin-like growth factor-binding protein 5 (Igfbp5) affects the synthesis and release of ECM through the MAPK signaling pathway, further affecting bladder detrusor fibrosis [20]. Synapsin-2 (Syn2) is involved in presynaptic membrane neurotransmitter release [21], and ATP synthase subunit g, mitochondrial (Atp5l) affects smooth muscle contraction by affecting mitochondrial ATP synthesis [22].

In bladder neck, we found that ARF GTPase-activating protein GIT2 (GIT2) and protein piccolo (PCLO) are involved in neurotransmitter release from the AZs of the presynaptic membrane [23, 24], G protein signaling 6 (Rgs6) affects the contraction of smooth cells by regulating AC/cAMP/MLCK/MLC signaling pathways [25], protein kinase A-anchored protein 13 (Akap13) affects the contraction of smooth cells by regulating Rho/Rock/MLCP/MLC signaling pathways [26], Calcium-activated potassium channel subunit beta-1 (Kcnmb1) affects bladder smooth muscle contraction [27], 1-phosphatidylinositol 4,5-bisphosphate phosphodiesterase beta-3 (Plcb3) regulates the opening of Large-Conductance Calcium-Activated Potassium Channels (BKca) [28], Smtn (smoothelin) affects muscle functionality and increases extracellular matrix deposition [29]. Therefore, based on the literature review, we randomly selected two DEPs (Col4a2 and Gnaz) from the detrusor and two DEPs (Smtn and Kcnmb1) from the bladder neck for WB validation, with the selected proteins representing differential expression patterns observed in their respective tissue groups.

In the detrusor, compared with sham group, the expression level of Col4a2 in DBND group was significantly increased ($P < 0.05$), while the expression level of Gnaz was decreased ($P < 0.05$). After EA intervention, the expression level of Col4a2 was significantly reduced ($P < 0.05$) and Gnaz was increased ($P < 0.05$). In the bladder neck, compared with sham group, the expression levels of Smtn and Kcnmb1 in DBND decreased ($P < 0.01$) (Figure 4A – 4C). After EA intervention, the expression of Smtn and Kcnmb1 was increased ($P < 0.01$ and $P < 0.05$, respectively) (Figure 4D – 4F). Thus, the WB results of

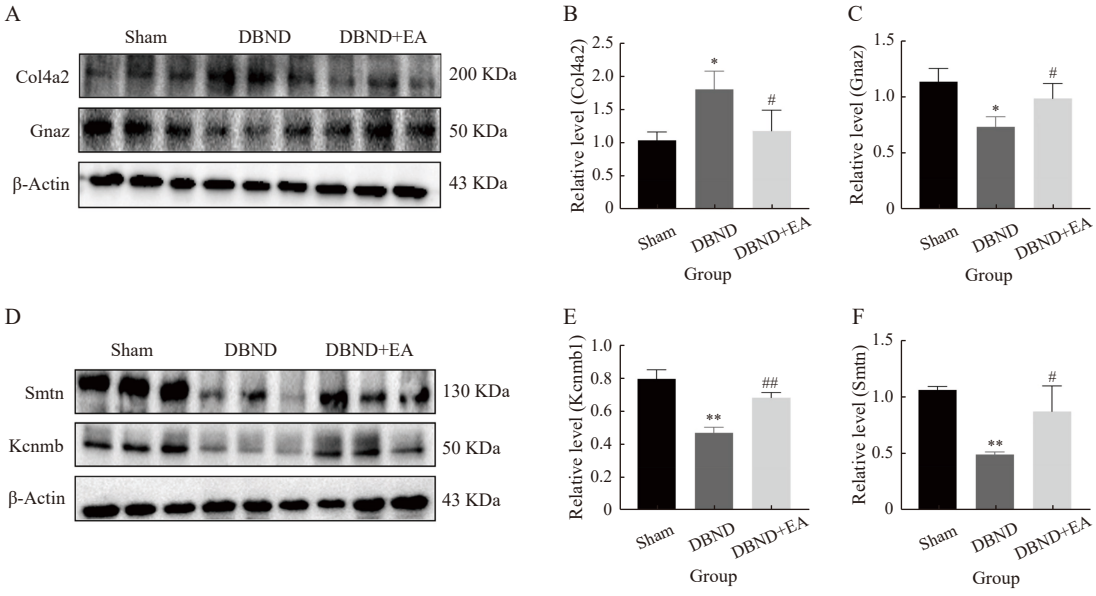

Figure 4 Validation of TMT quantitative proteomic analysis results by WB

A, WB images of Col4a2 and Gnaz in detrusor tissue. B, quantification of Col4a2 expression level in detrusor. C, quantification of Gnaz expression level in detrusor. D, WB images of Smtn and Kcnmb1 in bladder neck tissue. E, quantification of Kcnmb1 expression level in bladder neck. F, quantification of Smtn expression level in bladder neck.

Col4a2 and Gnaz in the detrusor and Smtn and Kcnmb1 in the bladder neck were consistent with the TMT results. The data have been deposited in the ProteomeXchange database with the identifier PXD034595 (http://proteomecentral.proteomexchange.org/cgi/GetDataset?ID=PXD034595).

4 Discussion

4.1 Mechanism of EA-mediated improvement in DBND urinary function

Ciliao (BL32), a foot-Taiyang bladder meridian acupoint, regulates bladder dynamics via sacral "Qi transformation" and S2 – S4 neurostimulation. Its dual action enhances detrusor contraction (parasympathetic activation) and relaxes the bladder neck (nitric oxide pathways), aligning with traditional Chinese medicine (TCM)'s lower Jiao theory [30]. There are many records of acupuncture treating this disease in ancient Chinese medical books, and modern clinical studies validate EA's efficacy in neurogenic bladder [31]. Zhongji (RN3), the conception vessel's bladder alarm point (Mu-point), modulates bladder function through T12 – L1 spinal innervation. In TCM, it resolves lower Jiao Qi stagnation to alleviate bladder neck obstruction [32]. Clinically, Zhongji (RN3) acupuncture improves urodynamics (flow rate, residual volume) [33]. Sanyinjiao (SP6), a foot-taiyin spleen meridian acupoint, regulates detrusor hyperactivity through L4 – S3 spinal cord modulation, balancing hypogastric sympathetic and pelvic parasympathetic inputs [34]. Combined with Ciliao (BL32) and Zhongji (RN3), it synergistically activates S2 – S4 neural pathways to coordinate detrusor contraction and bladder neck relaxation [35] (Figure 5). This triad achieves bladder homeostasis via integrated sympathovagal regulation, embodying TCM's concept of Yin-Yang harmonization. Therefore, acupuncture at Zhongji (RN3), Sanyinjiao (SP6), and Ciliao (BL32) can regulate the sympathetic and parasympathetic nerves that innervate the bladder and simultaneously act on the detrusor and bladder neck, sequentially regulating the bladder function.

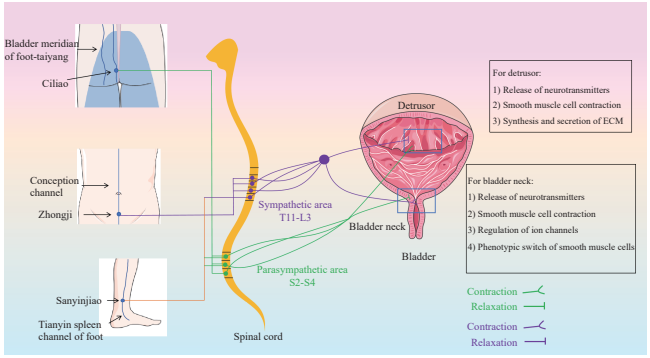

Figure 5 Schematic diagram of EA at Ciliao (BL32), Zhongji (RN3), and Sanyinjiao (SP6) for DBND meridian-acupoint neuroregulation-bladder function-therapeutic pathways

Our findings demonstrate that EA at Zhongji (RN3), Sanyinjiao (SP6), and Ciliao (BL32) significantly improved urinary dysfunction in DBND group. Post-EA intervention, MCC and LPP were reduced. HE analysis revealed alleviated detrusor edema, normalized smooth muscle fiber thickness, and decreased collagen deposition. Concurrently, the bladder neck exhibited diminished inflammatory infiltration and restored tissue architecture. These results align with prior evidence supporting EA's therapeutic efficacy in lower urinary tract dysfunction.

4.2 EA's mechanism of regulating detrusor muscle contraction revealed in proteomic and bioinformatic analysis

Another of the 30 DEPs, Phosphorylated Syn2 separates from synaptic vesicles to promote vesicle exocytosis, chemical synaptic signal transmission and neurotransmitter release [21] (Figure 6A). In Syn2 knockout mice, defective short-term synaptic plasticity disrupts neural signal coordination between bladder sensory and motor pathways [36]. Atp5l drives cellular energy production while suppressing cAMP to enhance detrusor contractility [37] (Figure 6B). EA upregulates Atp5l to improve ATP synthesis, strengthening detrusor contractility and bladder voiding efficiency [22]. Gnaz attenuates detrusor fibrosis and enhances contraction via cAMP suppression [38]. Studies have shown that cAMP can regulate smooth muscle cell contraction by activating the PKA/Pho/Rock/MLC pathway [19]. Gnaz blocks mirabegron's activation of β3-adrenoceptors, reducing excess cAMP to enhance detrusor contraction [39]. Gnaz suppresses cAMP-PKA-mediated smooth muscle relaxation via AC inhibition,

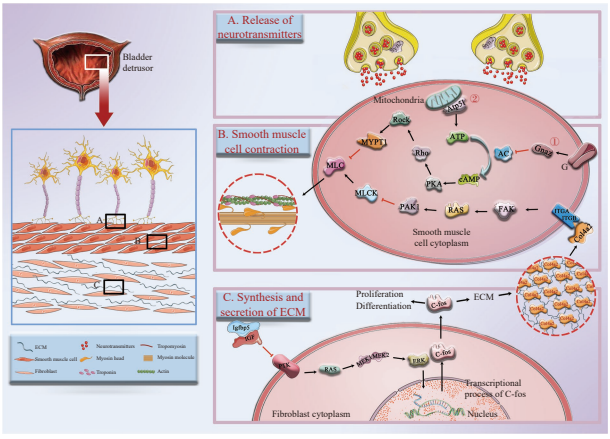

Figure 6 Potential association of EA-regulated 30 DEPs in bladder detrusor

A, Syn2's involvement in the release of neurotransmitters. B, Gnaz and Atp5l's association with the contraction of detrusor. ① Gnaz's effect on the contraction of detrusor. ② Atp5l's effect on detrusor contraction. C, Igfbp5's effect on detrusor fibrosis and Col4a2's effect on the contraction of detrusor.

modulating Rock/MLC pathways (Figure 6B). Our data revealed MAPK pathway enrichment in detrusor muscle, with Igfbp5 as the key DEP. Igfbp5 inhibits IGF signaling by dissociating IGF from its receptor, thereby suppressing IGF-mediated fibrosis via RAS/ERK cascades [20] (Figure 6C). EA treatment upregulated detrusor Igfbp5 while downregulating fibrotic markers Col4a2 and Fndc1. Col4a2 binding to integrins activates focal adhesion kinase (FAK)-RAC-serine/threonine protein kinase 1 (PAK1) signaling. The MLCK/MLC pathway is further regulated by activating in situ FAK to affect the contraction of smooth muscle cells [40] (Figure 6B). Our study found that Syn2, Atp5l, Gnaz, and Igfbp5 expression in DBND + EA group was increased compared with DBND group, while Col4a2 and PAK1 expression in DBND + EA group was decreased compared with DBND group. These findings suggest that targeting Syn2, Atp5l, Gnaz, Igfbp5, Col4a2, and PAK1 offers new treatment strategies for bladder disorders like overactive bladder or urinary retention.

4.3 EA mechanisms in bladder neck relaxation modulation unveiling in proteomic-bioinformatic analysis

The function of the bladder neck is related to neurotransmitters released by the nerve endings. The active zones (AZs) of the presynaptic membrane are the areas where synaptic vesicles bind to the presynaptic membrane to release neurotransmitters [41]. Among our enriched DEPs, Git2 and Pclo, as highly conserved proteins in AZs of the presynaptic membrane, participate in the presynaptic regulation of chemical synapses and affect the release of synaptic vesicles [42]. Studies have shown that Git2 can affect synaptic vesicle exocytosis by regulating actin cytoskeleton dynamics in AZs [23]. While Pclo negatively regulates the ubiquitination of proteins in AZs to protect synaptic cells and maintains synaptic integrity [24] (Figure 7A). In addition, we found that EA treatment upregulated Rgs6 and downregulated Akap13. Rgs6 enhances cAMP signaling by inhibiting Gnai-mediated AC suppression through GTPase activity [25], while Akap13 reduction attenuates RhoA/ROCK pathway activation, mitigating MLCP/MLC-mediated smooth muscle hypercontraction [26] (Figure 7B).

Bioinformatics analysis of the bladder neck showed that that the cGMP-PKG pathway and vascular smooth muscle contraction pathway were significantly enriched in the bladder neck [43]. Kcnmb1 and Plcb3 are the major DEPs engaged in these two pathways. Kcnmb1 potentiates BKca calcium sensitivity to inhibit smooth muscle contraction [44]. While Plcb3 stimulates Ca^{2+} mobilization via PLC/IP3 signaling, activating BK channels to induce relaxation [28] (Figure 7C). Our results validated EA-induced upregulation of Kcnmb1 and Plcb3 in bladder neck tissue compared to DBND group. In this way, EA upregulated bladder neck Kcnmb1 and Plcb3 expression, synergistically enhancing cGMP-PKG signaling to promote bladder neck relaxation.

Furthermore, our results show the relaxin signaling pathway was significantly enriched. The relaxin signaling pathway is closely related to fibrosis in various tissues, and fibrosis of bladder tissue ultimately affects smooth muscle contraction and bladder tissue compliance [45]. Chronic inflammation drives tissue fibrosis. Histomorphology revealed significant fibroblast and inflammatory cell infiltration in DBND group bladder necks, which was attenuated by EA treatment. Smtn downregulation during contractile-to-synthetic phenotypic transition correlates with reduced muscle functionality and increased extracellular matrix deposition, exacerbating tissue fibrosis [29] (Figure 7D). Post-surgical modeling significantly decreased bladder neck Smtn expression. EA intervention restored Smtn levels, demonstrating its capacity to stabilize contractile phenotypes and attenuate fibrotic remodeling, thereby preserving bladder function.

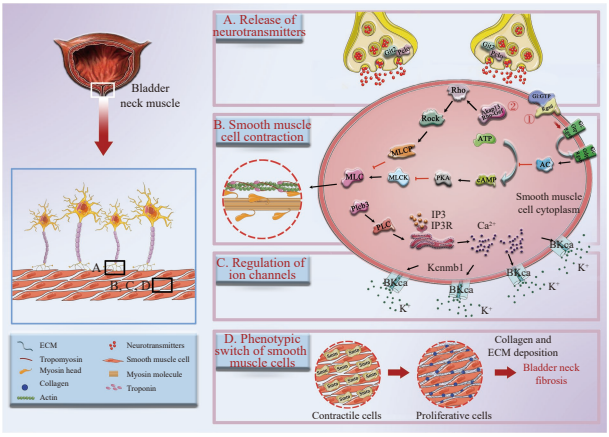

Figure 7 Potential association of EA-regulated 59 DEPs in the bladder neck

A, Git2 and Pclo's involvement in neurotransmitters release. B, Rgs6 and Akap13's involvement in the contraction of the bladder neck. ① Rgs6's involvement in the contraction of the bladder neck. ② Akap13's involvement in the contraction of the bladder neck. C, Plcb3's regulation of the opening of BKca channels. D, phenotypic switch of smooth muscle cells' effect on bladder neck fibrosis.

In this study, WB validated the expression of Col4a2, Gnaz, Smtn, and Kcnmb1, while the other DEPs discussed require further experimental confirmation. The study has several limitations: the absence of non-acupoint controls to establish the EA specificity, a female-only experimental design without assessment of estrous cycle effects, and the lack of investigation into potential sexual dimorphism. Future studies are planned to address these issues by incorporating sham electroacupuncture controls, testing both male or ovariectomized animal models, and validating key therapeutic targets through pharmacological interventions using specific agonists or inhibitors.

5 Conclusion

EA demonstrates dual therapeutic efficacy by differentially modulating detrusor and bladder neck pathophysiology. EA ameliorates fibrotic remodeling in detrusor and augments contractile function through coordinated regulation of MAPK signaling, focal adhesion complexes, and ECM-receptor interaction. Besides, EA modulates detrusor contraction through coordinated regulation of key molecular targets including Igfbp5, Gnaz, Syn2, and Atp5l to remodel extracellular matrix, regulate cAMP signaling, neurotransmitter release, and promote ATP biosynthesis. Concurrently, EA facilitates bladder neck relaxation by targeting fibrotic regulators (Smtn), ion channel modulators (Kcnmb1 and Plcb3), smooth muscle cells contraction (Rgs6 and Akap13) and synaptic plasticity mediators (Git2 and Pclo). This dual-tissue targeting strategy underscores the precision of EA in reprogramming biomolecular pathways to reinstate physiological bladder coordination between storage and voiding phases.

Fundings

National Natural Science Foundation of China (General Program, 81874510), Natural Science Foundation of Hunan Province (2022JJ40301), and Scientific Research Project of the Hunan Provincial Department of Education (21B0369).

Competing interests

The authors declare no conflict of interest.

References

[1] MILICEVIC S, SEKULIC A, NIKOLIC D, et al. Urinary tract infections in relation to bladder emptying in patients with spinal cord injury. Journal of Clinical Medicine, 2024, 13(13): 3898.

[2] CHEN YC, KUO HC. Risk factors of video urodynamics and bladder management for long-term complications in patients with chronic spinal cord injury. Scientific Reports, 2024, 14(1): 12632.

[3] KUO HC. Clinical application of botulinum neurotoxin in lower-urinary-tract diseases and dysfunctions: where are we now and what more can we do? Toxins, 2022, 14(7): 498.

[4] FURRER MA, KESSLER TM, PANICKER JN. Detrusor sphincter dyssynergia. The Urologic Clinics of North America, 2024, 51(2): 221–232.

[5] BIRKHÄUSER V, ANDERSON CE, KOZOMARA M, et al. Urodynamics are essential to predict the risk for upper urinary tract damage after acute spinal cord injury. Biomedicines, 2023, 11(6): 1748.

[6] LEI HZ, FU YN, XU GX, et al. Different types of acupuncture and moxibustion therapy for neurogenic bladder after spinal cord injury: a systematic review and network meta-analysis study protocol. Medicine, 2020, 99(1): e18558.

[7] CAO X, YU Z, XU B. Differences of bi-directional regulative effects between acu-moxibustion and Chinese materia medica interventions. Acupuncture Research, 2012, 37(5): 412–415.

[8] DONG LY, TAO X, GONG C, et al. Effects of central-peripheral FMS on urinary retention after spinal cord injury: a pilot randomized controlled trial protocol. Frontiers in Neurology, 2024, 14: 1274203.

[9] ZHONG P, ZENG H, HUANG MC, et al. Combined acupuncture and moxibustion therapy for the treatment of neurogenic bladder and bowel dysfunction following traumatic spinal cord injury: a case report. Explore, 2023, 19(1): 136–140.

[10] LIU Q, QU QR, XU M, et al. The protein kinase A signaling pathway mediates the effect of electroacupuncture on excessive contraction of the bladder detrusor in a rat model of neurogenic bladder. Acupuncture in Medicine, 2024, 42(1): 32–38.

[11] QU QR, TANG LY, LIU Q, et al. Proteomic analysis of the sphincter in a neurogenic bladder caused by T10 spinal cord injury. Journal of Integrative Neuroscience, 2022, 21(5): 147.

[12] SHAKER H, MOURAD MS, ELBIALY MH, et al. Urinary bladder hyperreflexia: a rat animal model. Neurourology and Urodynamics, 2003, 22(7): 693–698.

[13] SCHEFF SW, SAUCIER DA, CAIN ME. A statistical method for analyzing rating scale data: the BBB locomotor score. Journal of Neurotrauma, 2002, 19(10): 1251–1260.

[14] ZHENG Z, ZHANG L, ZHAO CC, et al. Identification of differentially expressed proteins in heart of mouse death from smother based on label-free proteomics. Legal Medicine, 2023, 65: 102302.

[15] KRAUZE AV, SIERK M, NGUYEN T, et al. Corrigendum: glioblastoma survival is associated with distinct proteomic alteration signatures post chemoirradiation in a large-scale proteomic panel. Frontiers in Oncology, 2024, 14: 1348105.

[16] PANG K, DONG Y, HAO L, et al. ERH interacts with EIF2α and regulates the EIF2α/ATF4/CHOP pathway in bladder cancer cells. Frontiers in Oncology, 2022, 12: 871687.

[17] MA YY, ZHANG GJ, LIU PF, et al. Comprehensive genomic analysis of puerarin in inhibiting bladder urothelial carcinoma cell proliferation and migration. Recent Patents on Anti-Cancer Drug Discovery, 2024, 19(4): 516–529.

[18] BOUCHAREB R, GUAUQUE-OLARTE S, SNIDER J, et al. Proteomic architecture of valvular extracellular matrix: FNDC1 and MXRA5 are new biomarkers of aortic stenosis. JACC Basic to Translational Science, 2021, 6(1): 25–39.

[19] KUMAR KP, WILSON JL, NGUYEN H, et al. Stroke alters the function of enteric neurons to impair smooth muscle relaxation and dysregulates gut transit. Journal of the American Heart Association, 2024, 13(3): e033279.

[20] GUO YY, XIAO YY, ZHU HY, et al. Inhibition of proliferation-linked signaling cascades with atractylenolide I reduces myofibroblastic phenotype and renal fibrosis. Biochemical Pharmacology, 2021, 183: 114344.

[21] RUNWAL GM, EDWARDS RH. The role of α-synuclein in exocytosis. Experimental Neurology, 2024, 373: 114668.

[22] LI X, HU JW, YIN P, et al. Mechanotransduction in the urothelium: ATP signalling and mechanoreceptors. Heliyon, 2023, 9(9): e19427.

[23] YOO SM, CERIONE RA, ANTONYAK MA. The Arf-GAP and protein scaffold Cat1/Git1 as a multifaceted regulator of cancer progression. Small GTPases, 2020, 11(2): 77-85.

[24] FASS DM, LEWIS MC, AHMAD R, et al. Brain-specific deletion

of GIT1 impairs cognition and alters phosphorylation of synaptic protein networks implicated in schizophrenia susceptibility. Molecular Psychiatry, 2022, 27(8): 3272–3285.

[25] BOSCH DE, JECK WR, SIDEROVSKI DP. Self-activating G protein α subunits engage seven -transmembrane regulator of G protein signaling (RGS) proteins and a Rho guanine nucleotide exchange factor effector in the amoeba Naegleria fowleri. Journal of Biological Chemistry, 2022, 298(8): 102167.

[26] CORDEIRO MITCHELL CN, ISLAM MS, AFRIN S, et al. Mechanical stiffness augments ligand-dependent progesterone receptor B activation via MEK 1/2 and Rho/ROCK-dependent signaling pathways in uterine fibroid cells. Fertility and Sterility, 2021, 116(1): 255–265.

[27] YAMANOUCHI D, KASUYA G, NAKAJO K, et al. Dual allosteric modulation of voltage and calcium sensitivities of the Slo1-LRRC channel complex. Molecular Cell, 2023, 83(24): 4555-4569.e4.

[28] OU G, KOMURA A, HOJO M, et al. Pharmacological study on the enhancing effects of U46619 on guinea pig urinary bladder smooth muscle contraction induced by acetylcholine and α,β-methylene ATP and the possible involvement of protein kinase C. Journal of Pharmaceutical Sciences, 2023, 153(3): 119–129.

[29] MATSUMOTO S, HANAI T, SHIMIZU N, et al. Effect of edaravone on ischemia/reperfusion injury in rat urinary bladder--changes in smooth muscle cell phenotype and contractile function. Aktuelle Urologie, 2010, 41(Suppl 1): S46-S49.

[30] LU JY, YING XW, CHEN XL, et al. Effects of electroacupuncture at different acupoints on the histomorphology of neurogenic bladder and the expression of hyperpolarization-activated cyclic nucleotide-gated channels in interstitial cells of Cajal in a rat model of suprasacral spinal cord injury. Annals of Palliative Medicine, 2020, 9(6): 3830–3838.

[31] KHASANAH N, DJAALI W, VIVENTIUS Y. Electroacupuncture therapy for urinary retention in an elderly patient. Medical Acupuncture, 2024, 36(2): 108–112.

[32] WILLIAMS CL, CURFMAN SE, LINDSLEY SR, et al. Inferior-medial dry needling at the thoracolumbar junction: a cadaveric study. International Journal of Sports Physical Therapy, 2024, 19(10): 1238–1243.

[33] EL KHOURY J, HERMIEU N, CHESNEL C, et al. Primary bladder neck obstruction in men: the importance of urodynamic assessment and cystourethrography in measuring its severity. Neurourology and Urodynamics, 2024, 43(4): 874–882.

[34] GUO XL, LIU XN, WANG FC. Clinical application and mechanism of Sanyinjiao. Jilin Traditional Chinese Medicine, 2011, 31(1): 47–48.

[35] ZHU B. Correspondence between the running course of meridians and body segments. Acupuncture Research, 2021, 46(10): 815–820.

[36] BRUENTGENS F, MORENO VELASQUEZ L, STUMPF A, et al. The lack of synapsin alters presynaptic plasticity at hippocampal mossy fibers in male mice. eNeuro, 2024. doi: 10.1523/ENEURO.0330-23.2024.

[37] ARESTA BRANCO MSL, PERRINO BA, MUTAFOVA-YAMBOLIEVA VN. Spatial mapping of ectonucleotidase gene expression in the murine urinary bladder. Frontiers in Physiology, 2023, 14: 1306500.

[38] ZOU W, YU Q, MA Y, et al. Pivotal role of heterotrimeric G protein in the crosstalk between sugar signaling and abiotic stress response in plants. Plant Physiology and Biochemistry, 2024, 210: 108567.

[39] MUDERRISOGLU AE, CIOTKOWSKA A, RUTZ B, et al. Dynamic phenotypic shifts and M2 receptor downregulation in bladder smooth muscle cells induced by mirabegron. Frontiers in Pharmacology, 2024, 15: 1446831.

[40] ZHANG W, BHETWAL BP, GUNST SJ. Rho kinase collaborates with p21-activated kinase to regulate actin polymerization and contraction in airway smooth muscle. Journal of Physiology, 2018, 596(16): 3617-3635.

[41] CUNNINGHAM KL, LITTLETON JT. Mechanisms controlling the trafficking, localization, and abundance of presynaptic Ca^{2+} channels. Frontiers in Molecular Neuroscience, 2022, 15: 1116729.

[42] GUNDELFINGER ED, KARPOVA A, PIELOT R, et al. Organization of presynaptic autophagy-related processes. Frontiers in Synaptic Neuroscience, 2022, 14: 829354.

[43] LU Y, ZHANG X, HU W, et al. The Identification of candidate biomarkers and pathways in atherosclerosis by integrated bioinformatics analysis. Computational and Mathematical Methods in Medicine, 2021, 2021: 6276480.

[44] ZHOU Y, ZHANG F, JIANG H, et al. Fumaric acid and succinic acid treat gestational hypertension by downregulating the expression of KCNMB1 and TET1. Experimental and Therapeutic Medicine, 2021, 22(4): 1072.

[45] WEIN AJ. Re: Fibrosis and the bladder, implications for function ICI-RS 2017. Journal of Urology, 2019, 201(6): 1060.

电针治疗骶上脊髓损伤后逼尿肌-膀胱颈协调障碍的蛋白质组学机制

唐丽亚[a†], 瞿启睿[a†], 刘锦灿[a], 许明[a], 周璐[b], 刘琼[a], 艾坤[a*]

a. 湖南中医药大学针灸推拿康复学院, 湖南 长沙 410208, 中国
b. 郴州第一人民医院康复医学科, 湖南 郴州 423000, 中国

【摘要】目的 阐明电针治疗骶上脊髓损伤后逼尿肌-膀胱颈协调障碍（DBND）的潜在机制。**方法** 将 52 只无特定病原体（SPF）级雌性 SD 大鼠（10 – 12 周龄，250 – 280 g）随机分为假手术组（$n = 12$）和脊髓损伤造模组（$n = 40$）。造模组采用 Hassan Shaker 法在 T10 水平行脊髓横断术建立 DBND 模型，符合标准的 24 只大鼠随机分为 DBND 组（$n = 12$）和电针干预组（DBND + EA 组，$n = 12$）。脊髓休克恢复后（造模后第 19 天），DBND + EA 组接受电针治疗，取次髎（BL32）、中极（RN3）、三阴交（SP6）穴位，每次 20 分钟，频率 10/50 Hz，每日 1 次，连续 10 天。假手术组和 DBND 组仅给予麻醉而不进行电针干预。造模后第 29 天，所有大鼠进行尿动力学检测，随后对逼尿肌和膀胱颈组织进行苏木精-伊红（HE）染色、串联质量标签（TMT）蛋白质组学和蛋白质印迹法（WB）分析。差异表达蛋白（DEPs）定义为 $P < 0.05$、唯一肽段≥2、倍数变化> 1.2 或< 0.83 的蛋白质。采用 KOBAS 3.0 进行京都基因与基因组百科全书（KEGG）通路分析（$P < 0.01$），使用基因/蛋白质相互作用检索工具（STRING）11.5 和 Cytoscape 3.9.1 构建蛋白质-蛋白质相互作用（PPI）网络。**结果** 与假手术组相比，DBND 组的漏点压力（LPP）和最大膀胱测压容量（MCC）均显著升高（均为 $P < 0.01$）。与 DBND 组相比，电针治疗显著降低了 LPP 和 MCC（分别为 $P < 0.01$ 和 $P < 0.05$）。HE 染色显示电针减少了逼尿肌纤维化并改善了膀胱颈炎症。TMT 蛋白质组学在逼尿肌中鉴定出 30 个重叠 DEPs，在膀胱颈中鉴定出 59 个重叠 DEPs（通过比较 DBND + EA 组与 DBND 组相对于假手术组的差异）。在逼尿肌组织中，KEGG 分析显示 10 条通路显著富集（$P < 0.01$），包括丝裂原活化蛋白激酶（MAPK）信号通路。PPI 分析显示 30 个 DEPs 中有 22 个相互关联。在膀胱颈组织中，14 条通路显著富集（$P < 0.01$），包括松弛素信号通路，59 个 DEPs 中有 51 个显示相互关联。TMT 和 WB 验证均表明，与假手术对照相比，DBND 大鼠逼尿肌组织中 IV 型胶原 α2 链（Col4a2）表达上调，鸟苷酸结合蛋白 G(z) 亚基 α（Gnaz）表达下调，而电针治疗使这两个蛋白表达正常化（均为 $P < 0.05$）。在膀胱颈组织中，与假手术对照相比，DBND 大鼠的平滑肌蛋白（Smtn）和钙激活钾通道 β1 亚基（Kcnmb1）表达下降（均为 $P < 0.01$），电针治疗后两者表达均上调（分别为 $P < 0.01$ 和 $P < 0.05$）。**结论** 电针通过双靶点机制恢复 DBND 中的逼尿肌-膀胱颈协调功能。在逼尿肌组织中，电针通过细胞外基质重塑、环磷酸腺苷（cAMP）信号调节以及神经递质介导的三磷酸腺苷（ATP）生物合成增强来调节收缩功能。在膀胱颈组织中，电针通过维持收缩表型、减少纤维化、抑制平滑肌兴奋性以及调节突触前神经递质释放来促进松弛。这些发现为电针治疗 DBND 的机制提供了新的见解。

【关键词】电针；骶上脊髓损伤；逼尿肌-膀胱颈协同失调；逼尿肌；膀胱颈；蛋白质组学分析；差异表达蛋白